inventions

MDPI

Article

Design and 3D Manufacturing of an Improved Heliostatic Illuminator

Marta Varo-Martínez, José C. Ramírez-Faz, Jesús López-Sánchez, Manuel Torres-Roldán, Luis Manuel Fernández-Ahumada * and Rafael López-Luque

Physics for Energy and Renewable Resources Research Group, Campus of Rabanales, University of Cordoba, 14071 Cordoba, Spain

* Correspondence: lmfernandez@uco.es

Abstract: Increasing daylighting levels contributes to improving the energy efficiency of buildings and consequently to the fight against climate change. This work presents a new illuminator based on a previous single-axis polar heliostat. This heliostat allows redirecting sunlight to a specific space to be illuminated at any time of the day. The system presented is simple but compact in size. It has been manufactured by 3D printing with recyclable PETG plastics. Three-dimensional printing has allowed reduction of the mass of the system to less than 5 kg, which means high stability and manageability. Moreover, the system has been provided with an assembly structure that facilitates its correct installation by a single operator. The result is a heliostatic illuminator with an average pointing error of 10 mrad, an acceptable error for urban applications. Finally, a low-cost and high-replicability device has been achieved, which makes it an easily reproducible illuminator and favors its extensive installation.

Keywords: heliostat; daylighting; energy efficiency; energy saving

Citation: Varo-Martínez, M.; Ramírez-Faz, J.C.; López-Sánchez, J.; Torres-Roldán, M.; Fernández-Ahumada, L.M.; López-Luque, R. Design and 3D Manufacturing of an Improved Heliostatic Illuminator. *Inventions* **2022**, *7*, 127. https://doi.org/10.3390/inventions7040127

Academic Editors: Craig E. Banks

Received: 25 November 2022
Accepted: 14 December 2022
Published: 19 December 2022

1. Introduction

Nowadays, there is scientific consensus that climate change is an evident reality involving serious consequences for the Earth, for socio-economic systems, and for human health itself [1]. There is also consensus regarding the main cause of climate change being the emission of greenhouse gases derived from human activity (use of energy from fossil fuels, industrial processes, transportation, agriculture, etc.) [2]. For these reasons, in 1979 the first World Climate Conference identified climate change as an urgent global problem requiring joint action by governments and institutions worldwide [3]. In this regard, in 1992, countries around the world agreed on the "United Nations Framework Convention on Climate Change" to develop initiatives and proposals to promote the mitigation of climate change [4]. Since then, several conventions to define specific objectives and commitments have been held. Among the various meetings held, the COP21 in Paris was a milestone in terms of the agreements adopted [3] because members committed to: (i) keep the global temperature increase below 2 °C, continuing efforts to limit it to only 1.5 °C; (ii) promote development with low greenhouse gas emissions; and (iii) direct financial flows to achieve climate-sensitive, low-emission development [5]. Recently, the Intergovernmental Panel on Climate Change (IPCC) in its 2022 report indicated that it is still possible to limit the global temperature increase to 1.5 °C as long as governments engage with a strong political determination to increase climate ambition [6].

At the European level, climate change policies are framed in the context of The European Green Deal [7]. The aim of this deal is to promote measures to achieve a climate-neutral, modern, and sustainable European Union (EU) by 2050. Among the measures

proposed, the EU and its Member States are committed to reducing the EU's net greenhouse gas emissions by at least 55% compared to 1990 levels by 2030.

In addition, the war in Ukraine has highlighted the EU's high dependence on fossil fuel imports and the risks this entails for the economy [8]. Specifically, at a global level, the EU imports 40% of the gas it consumes from Russia, though this percentage varies from one country to another [9]. As a consequence, facing the threat of supply cuts from Russia, the EU has been forced to accelerate the change of the energy model in order to reduce dependence on Russian fossil fuels.

For all these reasons, the EU is engaged in an accelerated process of changing the energy system. In that sense, promoting renewable energies is on its own insufficient and additional actions by governments and society are required to reduce energy consumption and to improve energy efficiency.

In this regard, Directive 2012/27/EU on energy efficiency indicates that 40% of final energy consumption in the European Union corresponds to energy consumption in buildings [10]. Specifically, artificial lighting is one of the most energy-intensive loads in buildings [11–16]. Consequently, increasing the use of natural lighting in buildings is one of the main actions to reduce their energy consumption and improve their efficiency [16–19]. In addition, the use of natural light as a source of illumination also provides other important advantages, including the improvement of the occupants' well-being [15,16,18,20–23].

Traditionally, daylighting systems have been vertical (windows) or horizontal (skylights) openings in building walls. However, these systems are affected by the high density and height of buildings in urban environments, which prevent the access of sunlight to their insides [24]. Furthermore, the optimization of the terrain has led to an increase in the use of subway or interior spaces without horizontal or vertical openings providing access to sunlight [25]. Therefore, in recent years different technological devices have been developed to improve the levels of natural lighting in buildings. In line with this, several authors have demonstrated the usefulness of passive illuminators that take advantage of incident irradiance and redirect it towards the interior of the spaces to be illuminated, such as light shelves [17,26] or light pipes [27–33]. In contrast to these passive devices, active illuminators take this a step further and try to increase the levels of solar irradiance that will be used for natural lighting by means of concentration or solar tracking. Among the active systems, fiber daylighting is usually composed of an initial solar radiation collection system with or without solar tracking, a fiber optic cable that transports the collected light to the space to be illuminated, and a final system that distributes the light [23]. The main advantages of this system over light pipes are its flexibility and easier installation, as well as its greater reach (20–50 m). However, due to multiple reflections, the light is attenuated along its path through the optical fiber [34]. Alternatively, heliostats have a much longer transmission distance of up to several kilometers and can therefore be very useful for building illumination [23].

Heliostats are systems that allow sunlight to be redirected towards a certain space thanks to a system of mirrors that follow the movement of the Sun. In addition, heliostats act as a constant source of natural lighting throughout the day as long as there is solar availability [35]. Given these advantages, despite being one of the most complex illuminators [36] and their high cost [37], in recent years attempts have been made to develop daylighting systems based on heliostats. For example, Tsangrassoulis et al. [38] proposed an illuminator capturing solar irradiance using heliostats and Fresnel lenses and redirecting it to the space to be illuminated using fiber optics. Similarly, Bystronski et al. [25] have proven, using a scale model, that heliostats can improve the effectiveness of light pipes as daylighting systems. On the other hand, Whang et al. [39] proposed an active illuminator consisting of a heliostat and a modular mirror system that achieves uniform illumination in the plane. Akhadovet al. [40] presented a study based on multiple heliostats to illuminate underground spaces considering the Sun's motion and avoiding light losses. Ullah [41] introduced an interesting concept (multi-floor building is illuminated by concentrating and delivering sunlight to five floors) achieving an efficiency of 40% with uniform

illumination in the interior. There is also remarkable work developed by Yanpavlis et al. [42], demonstrating that a good selection of orientation angles in heliostats can increase the operation time period of the solar receivers by 20%. The way in which heliostats are arranged presents a challenging goal when natural illumination is required. Thus, a matrix of mirror array-based heliostat [43] can increase the average efficiency of a traditional heliostat by 3.32 times. It is shown that a correct design and implementation of heliostat-based lighting systems generates an increase in the efficiency of such systems [44].

Likewise, Torres-Roldán et al. [45] developed a simple and low-cost single-axis polar heliostat prototype. They simulated its pointing error under different orientation conditions, validating its effectiveness as a natural illumination device in buildings [46,47]. Moreover, by means of a scale reproduction of the system, they studied its possible application in educational spaces with poor natural lighting [46]. Specifically, they proved that the installation of heliostatic illuminators reduces the use of artificial lighting, resulting in energy savings of up to 64% [47].

However, a detailed analysis of the heliostat proposed by Torres-Roldán et al. [45] shows that the device presents defects that hinder its application in large-scale buildings. These limitations are insufficient protection of the mechanisms against the weather, difficulties for its fixation and correct alignment with the Earth's axis, excessive weight, and clearances in the mechanical joints that generate pointing errors. Consequently, this work describes a new version of this device in which, thanks to engineering advances, these deficiencies have been corrected.

Moreover, in recent decades, industry is undergoing a new revolution based on its digital transformation [48]. Together with the incorporation of flexible, intelligent, and autonomous technological solutions, efficiency and sustainability have dramatically increased [49]. Three-dimensional printing is one of the technologies favoring this advance towards the so-called Industry 4.0 [50]. Three-dimensional printing favors not only the manufacturing process of a component but also the previous design phase and the subsequent phase of incorporating improvements. Specifically, with regard to the design and manufacture of parts, it avoids resorting to traditional prototyping based on mock-ups or molds [51,52]. Three-dimensional printing is revolutionizing production systems, reducing manufacturing, assembly, and post-processing times and costs and the need for expensive tooling and fixtures [51–53]. In addition, 3D printing gives flexibility to production systems, allowing them to adapt to market demands [50,52]. Furthermore, it enables and reduces the cost of customization of the final products, as it does not require expensive molds designed and manufactured for this purpose [54–56]. Finally, 3D printing involves less raw material consumption and less waste generation, thus contributing to a more sustainable industrial model [51]. For all these reasons, its industrial expansion together with the research developed have favored the rapid progress of 3D printing technology. The number of technologies and materials being used has improved and increased, increasing the possible applications [39,57]. In fact, 3D printing is already essential in sectors such as automotive, healthcare, industrial equipment, education, and architecture, among others. [58,59]. In this context, the improved version of the heliostatic illuminator presented in this work has been manufactured by means of 3D printing techniques, thus achieving significant improvements in comparison to the prototype of Torres-Roldán et al. [45]. In addition, this improved heliostatic illuminator contributes to deepening the optimization of the design and implementation of daylighting devices based on heliostats, such as the ones previously described.

Accordingly, after this introduction contextualizing the work developed, Section 2 "Materials and Methods" describes the fundamentals of the heliostat performance and the manufacturing process of the heliostat by 3D printing. Subsequently, in Section 3, the characteristics of the different parts that make up the system are described. In Section 4, the main improvements achieved in the new version of the heliostat are discussed together with an analysis of the pointing error of the proposed illuminator. Finally, in Section 5, a summary of the main conclusions of this work is presented.

2. Materials and Methods

This section describes the geometrical and mechanical fundamentals of the single-axis polar heliostat, as well as its design and manufacturing process.

2.1. Astronomical Device Fundamentals

A heliostat is a device designed to redirect solar radiation to a predetermined target point. For this purpose, the motion of the heliostat must be based on the geometrical fundamentals of the Earth–Sun motion described by means of the solar vector. The solar vector, $\vec{s}$, is a unit vector that, departing from the center of the Earth, points at all times to the position of the Sun. Equation (1) represents the vectorial expression of the solar vector in the equatorial reference system (Figure 1).

$$\vec{s} = s_x\vec{\imath} + s_y\vec{\jmath} + s_z\vec{k} = sin\,\Omega\,t\ \ cos\,\delta\,\vec{\imath} + cos\,\Omega\,t\,cos\,\delta\,\vec{\jmath} + sin\,\delta\,\vec{k}, \quad (1)$$

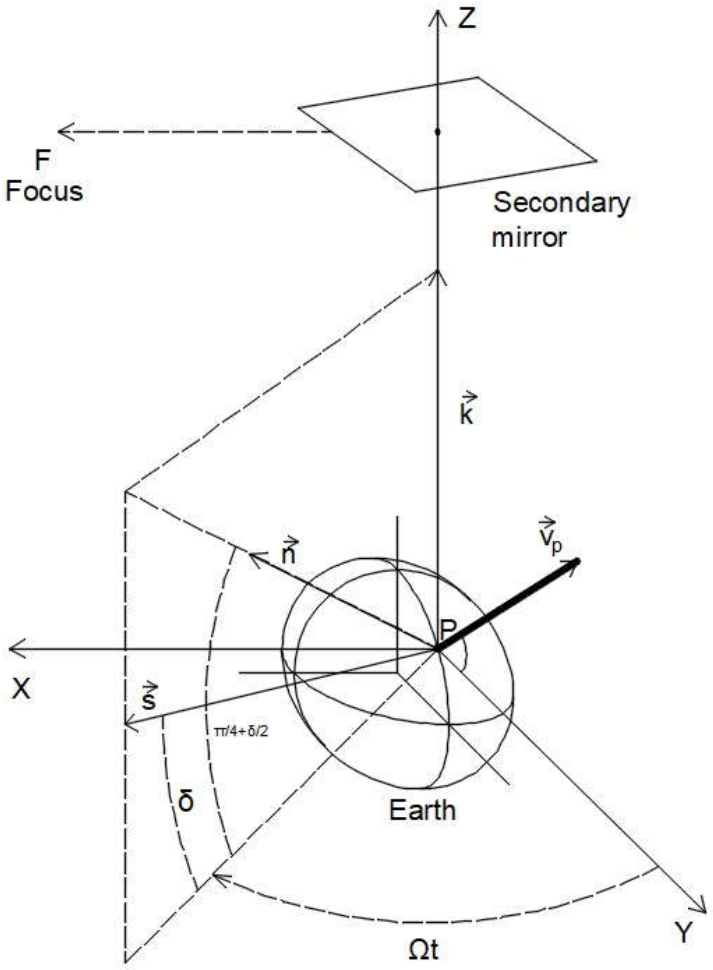

Figure 1. Astronomical fundamentals of heliostatic illuminator motion.

In Equation (1), δ is the declination, $\Omega = 2\pi/24\ rad/h$ is the angular velocity of the Earth in its translational motion, and t is the solar time measured from solar noon. Thus, t is a variable included in the interval (−12 h; 12 h), which is determined (in hours) by

Equation (2) in which GMT is the mean time at the Greenwich meridian, L is the longitude of the location considered (in degrees), and E_t is the equation of time, given by Equation (3).

$$t(h) = GMT + \frac{E_t}{60} + \frac{L}{15} - 12, \tag{2}$$

$$\begin{aligned} E_t(minute) = 229.18\Bigg[&0.000075 + 0.001868\,cos\left(\frac{2\pi(d_j-1)}{365}\right) \\ &- 0.032077 sin\left(\frac{2\pi(d_j-1)}{365}\right) - 0.014615\,cos\left(2\frac{2\pi(d_j-1)}{365}\right) \\ &- 0.04089 sin\left(2\frac{2\pi(d_j-1)}{365}\right)\Bigg], \end{aligned} \tag{3}$$

On the other hand, in Equation (1), δ represents the declination defined as the angle between the solar vector, $\vec{s}$, and the plane of the equator and is dependent on the Julian day, d_j, according to Spencer's model [60] given by Equation (4).

$$\begin{aligned} \delta(rad) = [&0.006918 - 0.399912\,cos\left(\tfrac{2\pi(d_j-1)}{365}\right) + 0.070257 sin\left(\tfrac{2\pi(d_j-1)}{365}\right) - \\ &0.006758\,cos\left(2\tfrac{2\pi(d_j-1)}{365}\right) + 0.000907 sin\left(2\tfrac{2\pi(d_j-1)}{365}\right) - \\ &0.002697\,cos\left(3\tfrac{2\pi(d_j-1)}{365}\right) + 0.00148 sin\left(3\tfrac{2\pi(d_j-1)}{365}\right)], \end{aligned} \tag{4}$$

Knowing the solar vector and, therefore, the direction of the solar rays, it is possible to determine the orientation that the mirror of the heliostat should have at each instant of time, i.e., the direction of the normal vector to the mirror, $\overrightarrow{n_a}$. For this purpose, it should be considered that, being a polar heliostat, the reflected rays should be directed in the direction parallel to the Earth's rotation axis, that is, the *z*-axis of the equatorial reference system (Figure 1). These rays reflected in the *z*-axis direction will be redirected towards the target focus, F, by means of a static secondary mirror (Figure 1). Therefore, according to the laws of reflection, $\overrightarrow{n_a}$ should be in the direction of the bisector of $\vec{s}$ and $\vec{k}$ (Figure 1). Thus, vector $\overrightarrow{n_a}$ should verify Equation (5).

$$\overrightarrow{n_a} = \frac{\vec{s}+\vec{k}}{|\vec{s}+\vec{k}|}, \tag{5}$$

Bearing in mind Equations (6) and (7) for $\vec{s}+\vec{k}$ y $\left|\vec{s}+\vec{k}\right|$, and substituting them in Equation (5), Equation (8) is obtained for normal vector to the mirror $\overrightarrow{n_a}$.

$$\vec{s}+\vec{k} = sin\,\Omega\,t\;\; cos\,\delta\,\vec{\imath} + cos\,\Omega\,t\,cos\,\delta\,\vec{\jmath} + (sin\,\delta+1)\vec{k}, \tag{6}$$

$$\left|\vec{s}+\vec{k}\right| = \sqrt{2+2\,sin\,\delta}\,, \tag{7}$$

$$\overrightarrow{n_a} = \frac{sin\,\Omega t\;\; cos\,\delta}{\sqrt{2+2\,sin\,\delta}}\vec{\imath} + \frac{cos\,\Omega t\,cos\,\delta}{\sqrt{2+2\,sin\,\delta}}\vec{\jmath} + \frac{(sin\,\delta+1)}{\sqrt{2+2\,sin\,\delta}}\vec{k}, \tag{8}$$

Considering trigonometrical equivalences (9) and (10), the normal vector is given at each instant by Equation (11):

$$\frac{cos\,\delta}{\sqrt{2+2\,sin\,\delta}} = cos\left(\frac{\pi}{4}+\frac{\delta}{2}\right), \tag{9}$$

$$\frac{1+sin\,\delta}{\sqrt{2+2\,sin\,\delta}} = sin\left(\frac{\pi}{4}+\frac{\delta}{2}\right), \tag{10}$$

$$\begin{aligned} \overrightarrow{n_a} = n_x\vec{\imath} + n_y\vec{\jmath} + n_z\vec{k} = sin\,\Omega\,t\;\; &cos\left(\frac{\pi}{4}+\frac{\delta}{2}\right)\vec{\imath} + cos\,\Omega\,t\,cos\left(\frac{\pi}{4}+\frac{\delta}{2}\right)\vec{\jmath} + \\ &sin\left(\frac{\pi}{4}+\frac{\delta}{2}\right)\vec{k}, \end{aligned} \tag{11}$$

Equation (11) allows one to verify that $\overrightarrow{n_a}$ is a unit vector completing each day, a rotation around the Earth's axis, Ω being the angular velocity of this rotation. Likewise,

for an adequate reflection of the Sun's rays in the direction of the Earth's axis of rotation, the angle formed by this vector with the equatorial plane each day is $\delta_n = \left(\frac{\pi}{4} + \frac{\delta}{2}\right)$. The subsequent sections are based upon this astronomical fact and show the development of the mechanism approximating the actual motion of a mirror to that described by Equation (11).

2.2. Mechanical Device Fundamentals

Figure 2 shows the schematic design of the proposed heliostat (Figure 2a) and its corresponding implementation (Figure 2b). As can be seen in both representations, the heliostat presented is based on the movement of a flat quadrilateral A'ABC and articulated at A, B, and C. A transmission chain of articulated bars is represented, starting at the rotating axis A'A. This axis will rotate thanks to the motor, M, and will transmit the rotation to the bar AB (fixed length a). This bar will transmit that rotation to the bar BC (fixed length b). As point C transmits the movement on a nut threaded on the hollow tube T (inside of which the axis A'A runs), the movement followed by point C is helical, typical of a peripheral point of a nut (Figure 3). In this way, the rotation of the motor, M, ensures not only that the whole mechanism A'ABC rotates around the axis A'A but also that the triangle ABC is deformed, because the distance AC varies as the rotation movement is produced. In addition, a mirror or primary reflector is placed on the bar AB so that the plane of this mirror is perpendicular to the plane of the mechanism ABC. In this way, the deformation of the polygon A'ABC, represented by the variation of the angle at vertex A, γ, results in a change of orientation of the mirror. As an example, Figure 4 shows the orientation of the heliostat primary mirror at two system positions that differ by a total number of 40 complete revolutions.

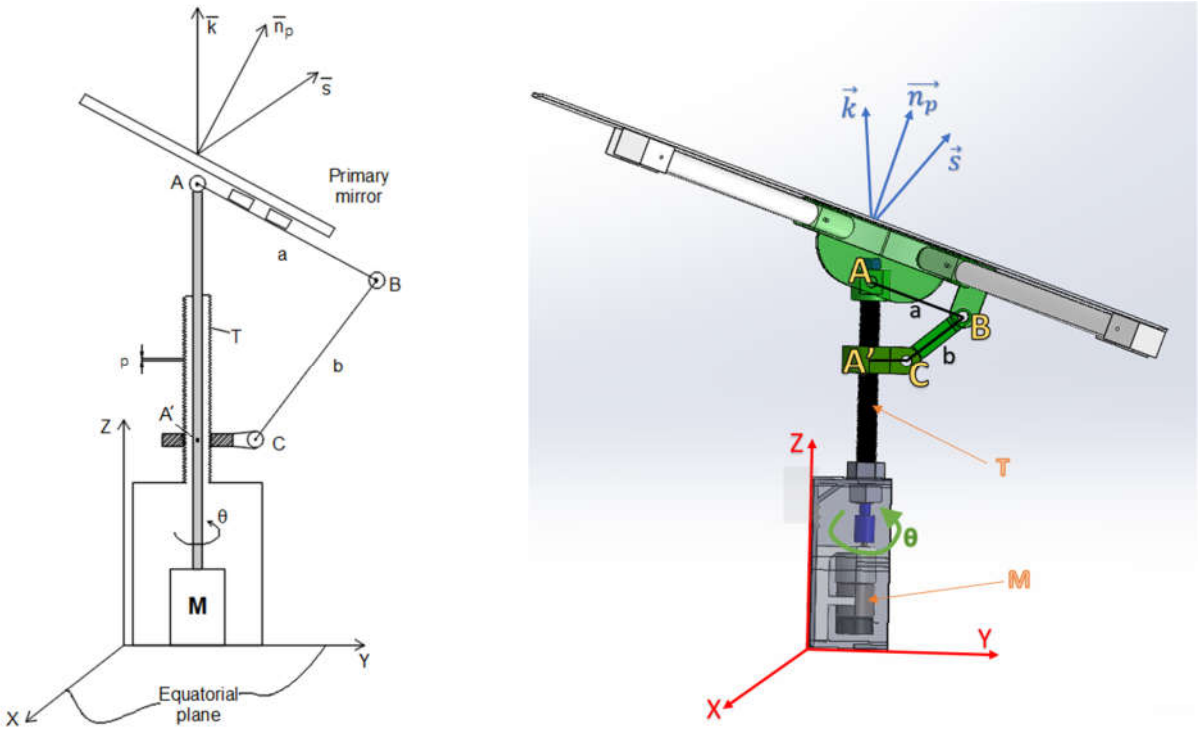

(**a**) (**b**)

Figure 2. (**a**) Schematic diagram of the mechanical operating principle for the proposed heliostat. (**b**) Significant measures for the proposed heliostat.

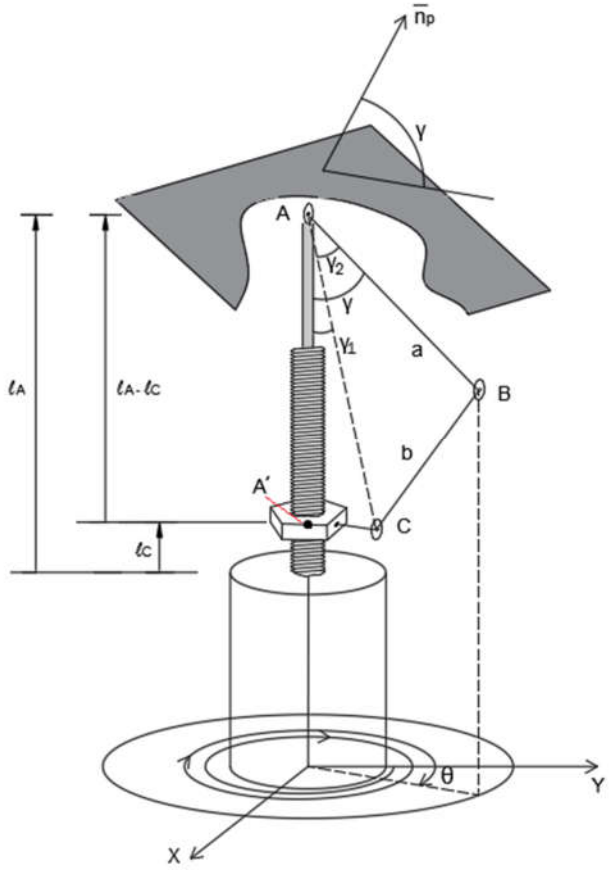

Figure 3. Schematic of the motion of the deformable polygon for the proposed heliostat.

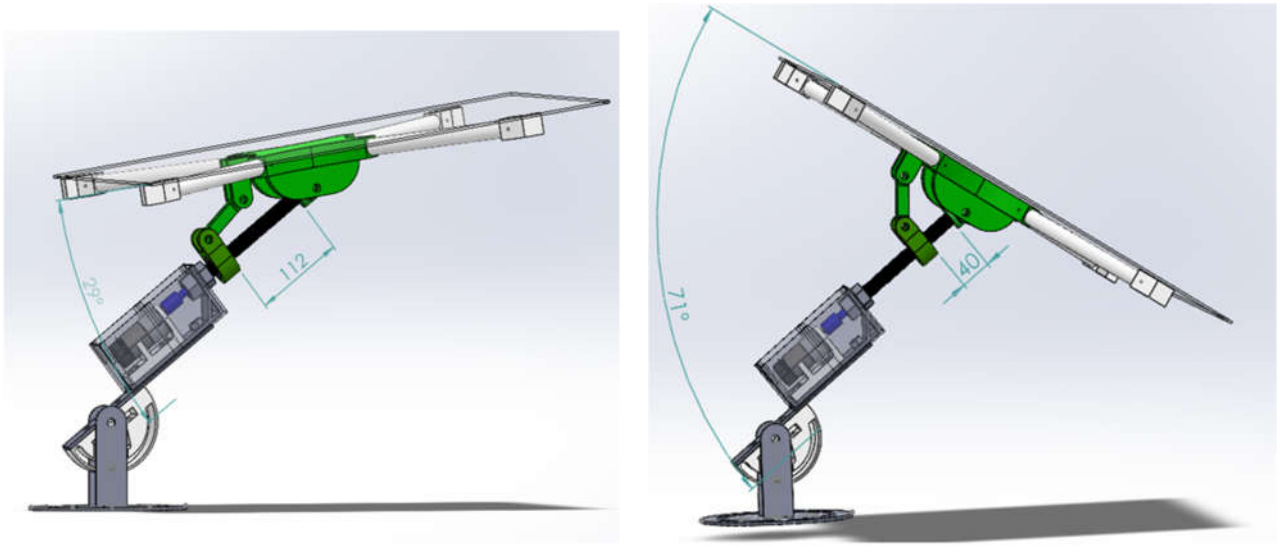

(**a**) (**b**)

Figure 4. Orientation of the heliostat primary mirror for two positions, (**a**) and (**b**), differing by 40 complete system revolutions.

Thus, adapting the angle γ to the angle δ_n, the heliostat redirects the Sun's rays to the desired fixed point. This deformation angle γ can be expressed as a function of the heliostat design variables (Figure 3) according to Equation (12).

$$\gamma = \gamma_1 + \gamma_2 = arctg\left(\frac{c}{l_A - l_C}\right) + arccos\left(\frac{b^2 - a^2 - c^2 - (l_A - l_C)^2}{2a\sqrt{c^2 + (l_A - l_C)^2}}\right), \quad (12)$$

In Equation (12), l_C represents the position of point C along the z-axis. Thus, when p is the pitch of the nut of the tube T, for a total angle of rotation of the plane of the deformable polygon θ, l_C will be given by Equation (13)

$$l_C = \frac{\theta}{2\pi} p, \quad (13)$$

On the other hand, from the deformation angle, γ, and Figure 3, one can extract, for a given rotation angle θ, the real direction of the normal vector to the heliostat primary mirror, $\overrightarrow{n_p}$, verified by Equation (14).

$$\overrightarrow{n_p} = sin\,\theta \cdot \; cos\,\gamma\,\vec{i} + cos\,\theta \cdot cos\,\gamma\,\vec{j} + sin\,\gamma\,\vec{k}, \quad (14)$$

According to the above, the heliostat pointing will be more accurate, the closer the directions of the vectors $\overrightarrow{n_a}$ and $\overrightarrow{n_p}$ are approximated. Thus, Figure 5 shows, as an example, the position of $\overrightarrow{n_p}$ on a unit sphere centered at P as the value of θ increases. In addition, the end point of $\overrightarrow{n_a}$ (Equation (11)) has been superimposed on this sphere as a shaded area. Figure 5 allows us to appreciate that the proposed mechanism, in general, will not be able to exactly match the mirror position, given by $\vec{n}_P$, to that of the ideal value according to the principles of astronomy, $\overrightarrow{n_a}$. Therefore, the system is designed and automated so that, at each time, the position offered by the heliostat $(\overrightarrow{n_p})$ is optimally close to the desired position $(\overrightarrow{n_a})$ given by Equation (11). However, in general, an approximation or pointing error will exist. These errors must be characterized and evaluated on a case-by-case basis.

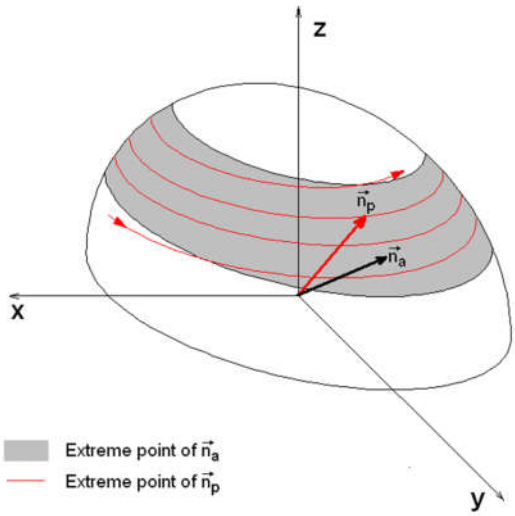

Figure 5. Graphical comparison between the possible positions for $\vec{n}_P$ and $\vec{n}$.

Finally, regarding the mechanical design of the device, it is important to highlight that the design of this type of device must consider the following limiting conditions:

1. The bar lengths must be allowed, for a summer solstice day, to have a value of θ, resulting in a value of $\gamma_{max} = \frac{\pi}{4} + \frac{\delta_{max}}{2} = 56.73$, according to Equations (12) and (13).

2. Similarly, for a winter solstice day, the value $\gamma_{min} = \frac{\pi}{4} - \frac{\delta_{max}}{2} = 33.27°$ must be achievable by the mechanism.
3. Finally, because the pointing error depends on the dimensions of the device, a thorough analysis of the pointing error must be performed. In addition, dimensions should be chosen to provide a manageable error for the intended application.

For the fulfillment of conditions 1 and 2, a geometrical construction of the bars in these extreme positions is recommended. Thus, the non-existence of geometrical incompatibilities would be observed. These diagrams are shown in Figure 6. Specifically, Figure 6a,b show valid configurations for the summer and winter solstices, respectively. However, the configuration shown in Figure 6c is not valid for the summer solstice because the length of bar BC (b) is too short with respect to the length of bar AB (a). Similarly, the configuration shown in Figure 6d is not valid for the winter solstice because the length of bar AB (a) is too short.

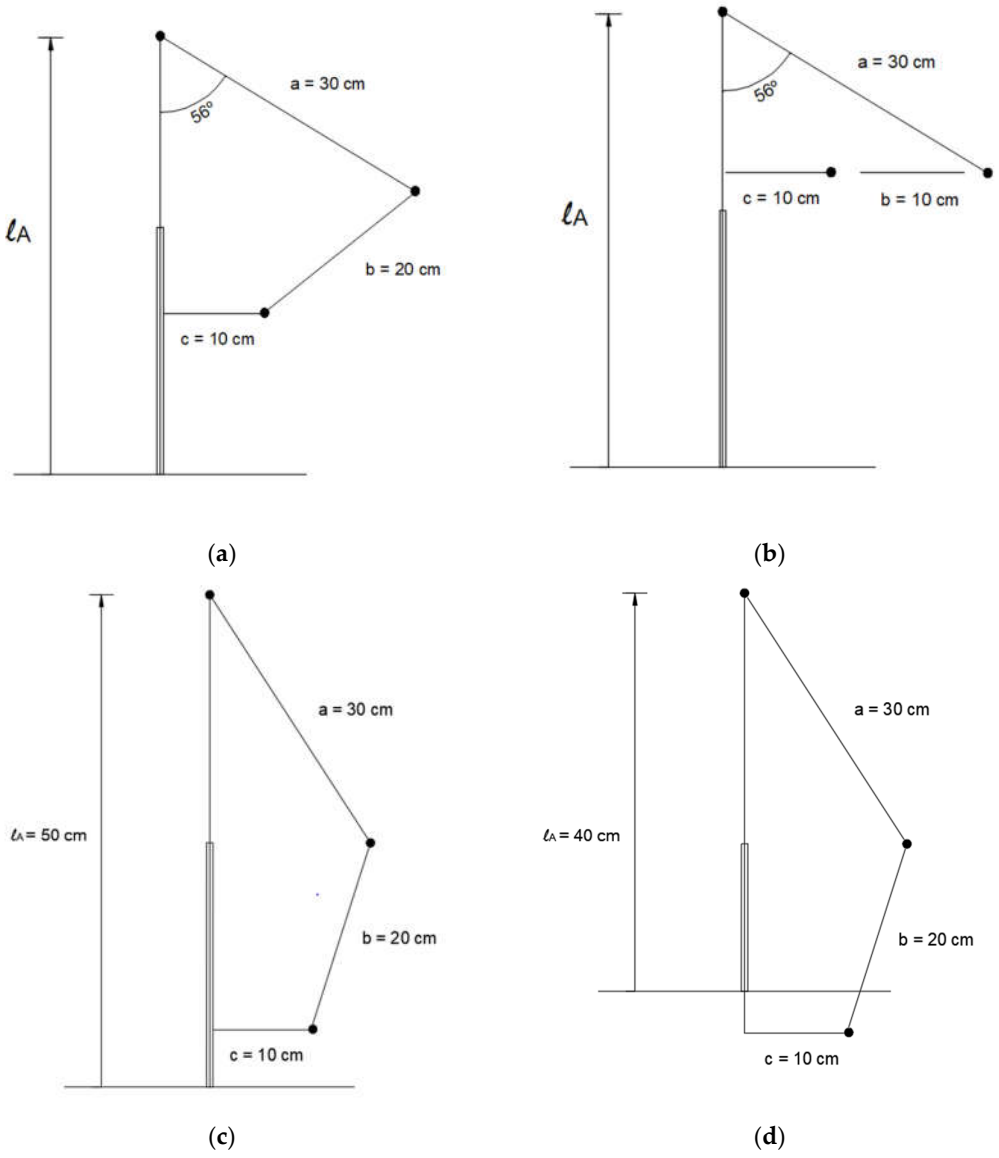

Figure 6. Graphical validity checks of the combinations of mechanical design variables for the proposed heliostat: (**a**) the represented combination meets the condition of positioning at the summer

solstice; (**b**) the represented combination meets the condition of positioning at the winter solstice; (**c**) the represented combination does not meet the condition of positioning at the summer solstice; (**d**) the represented combination does not meet the condition of positioning at the winter solstice.

2.3. Heliostat 3D Manufacturing

According to the advantages previously described, 3D printing has been used for the fabrication of the improved heliostat presented here. This facilitates manageability, replicability, adaptability, and a low manufacturing cost compared to the machining of metal parts. However, for the more mechanically demanding parts, steel has been used to avoid vibrations and lack of precision in the heliostat pointing.

The design of the heliostat has been made in such a way that it is feasible to be printed on any common FDM (Fused Deposition Modeling) 3D printer. Specifically, Table 1 shows the print settings used in this work for the illuminator manufacturing.

Table 1. Print settings for the FDM manufacturing of the proposed heliostatic illuminator.

Print Settings	Dimensions	Unit
Print Area	220 × 220 × 250	mm
Layer Height	0.2	mm
Nozzle	0.4	mm
Initial Layer Height	0.3	mm
Infill Density	30	%
Printing temperature	245	°C
Build Plate temperature	90	°C
Print speed	60	mm/s
Fan Speed	0	%
Support	Not needed	

As far as printing materials are concerned, there is nowadays a wide range of materials available. Thus, when choosing the printing material, it is advisable to consider its mechanical and physical properties in order to choose the material whose characteristics are best suited to the conditions of use of the product to be printed. In the case of the heliostat, it was necessary to choose a material that would behave well in conditions of high temperatures because of continuous exposure to sunlight. Moreover, the behavior of the material during printing is a key factor in the choice, because not all materials print equally easily. Additionally, it is important to note that most plastics available for 3D printing are 100% recyclable, which is an important advantage, especially when designing technological solutions that aim to improve the sustainability of our environment.

Accordingly, ABS, ASA, and PETG plastics are materials that could be optimal for the construction of the heliostat. However, the different tests performed showed that the parts made in ABS and ASA presented many printing problems and also did not meet the dimensional tolerances of the design. Therefore, PETG was finally used because the ease of printing and its dimensioning tolerance made it undoubtedly better in the overall computation of characteristics.

Finally, through 3D printing, flexibility has been achieved to incorporate and evaluate successive improvements until the final device is obtained. Economic and time costs have been reduced by not resorting to traditional prototyping. As an example, Figure 7 shows the simulation of the printing of the mirror base. As shown in the Figure, the final cost of the part is EUR 3.59, which is much lower than the cost of conventional machining.

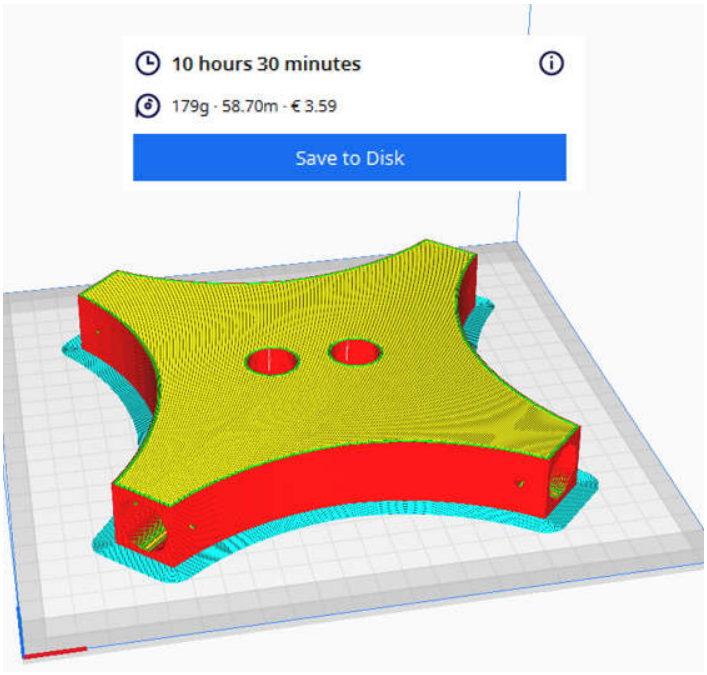

Figure 7. Simulation of mirror base printing.

3. Results

3.1. Proposed Heliostatic Illuminator

The designed system allows redirecting sunlight to a fixed point acting as a daylighting device in buildings. Table 2 shows the dimensions of the main design magnitudes of the heliostat illuminator.

Table 2. Main design features for the proposed heliostatic illuminator.

Features	Nomenclature	Length (mm)
Arm length	a	88.52
Pusher length	b	65.00
Separator length	c	33.50
Screw pitch	p	1.50

The different parts of the heliostat resulting from the design and manufacturing process are described in detail below.

3.1.1. Deformable Polygon

Figure 8 shows the parts that constitute the deformable polygon of the heliostat system on which the main mirror of the heliostat rests. The part has been manufactured by 3D printing in PETG (represented in green in Figure 8), except for the extensions between the tips and the base, which are made of aluminum to provide greater rigidity (represented in grey in Figure 8). This deformable polygon, according to the mechanical fundamentals described in Section 2.2, is in charge of properly orienting the mirror for correct solar tracking. For this purpose, the movement of the deformable polygon is articulated around the threaded tube T, with a pitch of 1.5 mm. This is an aluminum tube with a diameter of 20 mm and an inner hole of 10 mm. As explained above, this threaded tube T is responsible for supporting the entire deformable polygon. At the same time, the T tube constitutes the line of displacement of the points AA' of the deformable polygon in its solar tracking movement.

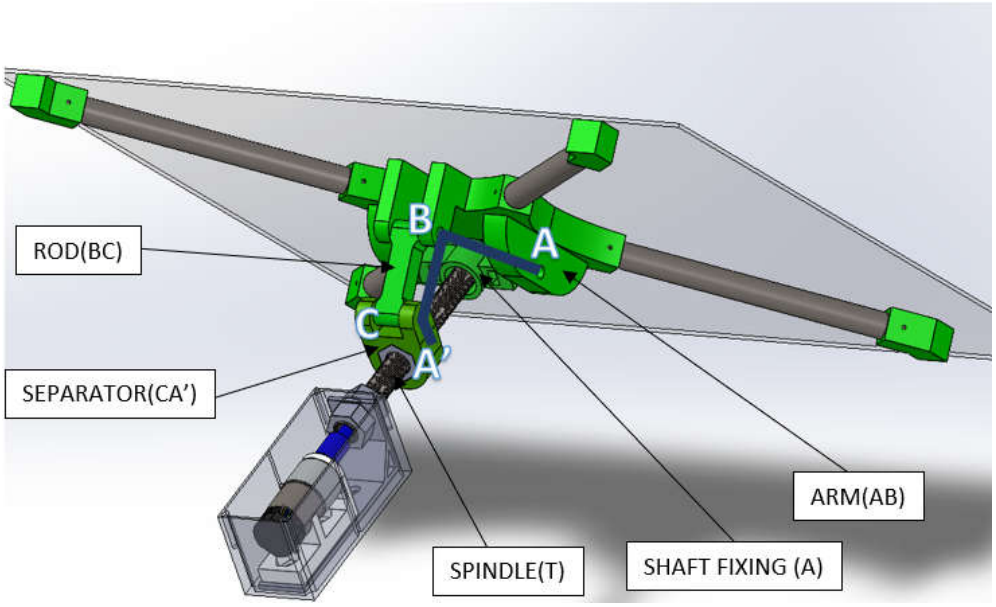

Figure 8. Deformable polygon for the proposed heliostatic illuminator.

3.1.2. Transmission Parts

The motion of the system is generated by a DC motor with encoder (Figure 9). The motor has a reduction ratio of 1:150 and provides a maximum torque of 6 Nm. In addition, the encoder has 2400 control points per revolution of the shaft, which allows the position of the heliostat to be precisely adjusted.

Meanwhile, the transmission consists of a 10mm threaded metal rod that moves inside the threaded tube T. The end piece of this transmission (in green in Figure 9) is attached to the deformable polygon, transmitting the movement to the whole system.

Finally, the coupler is the junction point between the transmission and the motor. It is made of plastic with 10 mm holes for the transmission and 6 mm holes for the motor shaft.

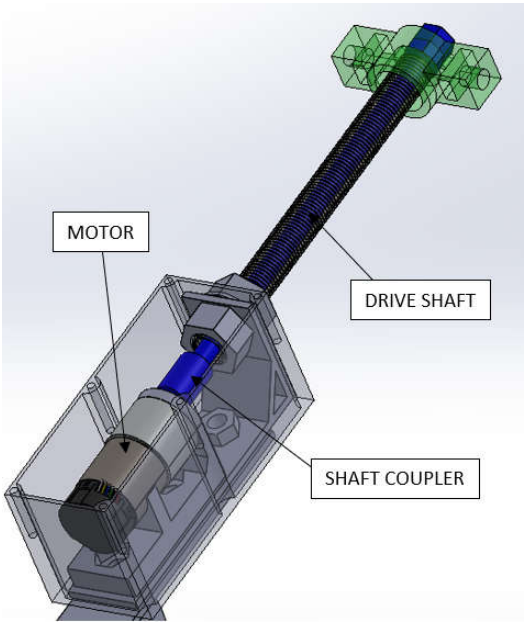

Figure 9. Transmission parts.

3.1.3. Support parts

As stated above, the heliostat should be oriented with its A'A axis parallel to the Earth's rotation axis. To facilitate accurate positioning and calibration, an adjustable bracket has been designed for both tilt and rotation on the horizontal plane (Figure 10). It consists of an L-shaped metal plate to which the T-tube is fixed by two nuts and a motor support made by 3D printing in PETG that is attached to the general support by two nuts.

The system also includes an angle adjuster, manufactured in PETG by 3D printing. This adjuster allows one to vary the inclination of the complete support. Consequently, the heliostat is tilted favoring its correct orientation in such a way that the angle formed by the A'A axis of the heliostat with the horizontal is equal to the latitude of the site.

Finally, the base of the support, made of 4 mm steel, is the junction point of the whole system with the place where the heliostat is installed. It has slots that provide the ability to vary the rotation to easily find the desired orientation.

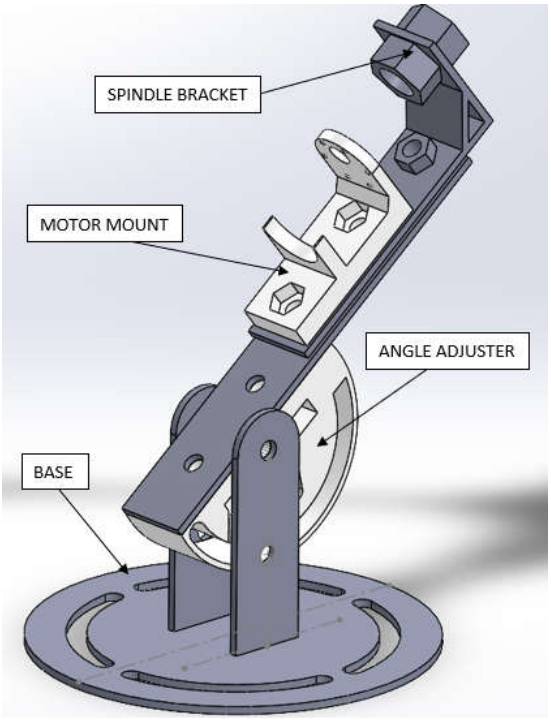

Figure 10. Support parts.

3.1.4. Installation Structure

For mounting and installation of the heliostat, a steel structure is used to support both the primary and secondary heliostat mirrors (Figure 11). This structure has been designed in such a way that the correct position of both mirrors can be easily adjusted. Specifically, the base on which the heliostat is fixed to the structure has the capacity to rotate 360 degrees. It also has bolts to adjust the height at four points so that it is completely levelled with the horizontal.

In addition, as mentioned above, the heliostat mount has an angle adjuster that allows the system axis (A'A) to be precisely positioned at the proper tilt so that the axis is parallel to the Earth's rotation axis. In this way, the Sun's rays reflected by the main mirror will be directed along this direction. Thus, by matching the center of the heliostat's secondary mirror with this direction and giving it the desired orientation, thanks to the spherical support that joins it to the structure, the solar radiation can be redirected towards the place to be illuminated.

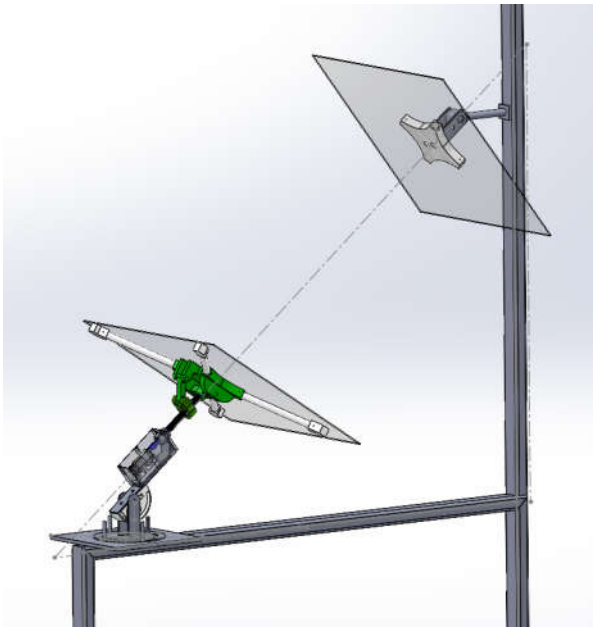

Figure 11. Device designed for mounting the proposed heliostatic illuminator.

Finally, in accordance with the description of the proposal, an economic valuation has been made of the proposed heliostat manufacturing costs, which are estimated to be less than EUR 250.

4. Discussion

4.1. Pointing Error Analysis

This section analyzes the pointing error of the device as a heliostat illuminator. For this purpose, it is assumed as a case study that the heliostat will be installed to illuminate a classroom with little direct access to the solar resource. It is located in the basement of the Albert Einstein building of the Rabanales campus of the University of Cordoba (Spain, latitude: 37.85° N; longitude: 4.18° W) (Figure 12).

Figure 12. Case study: Albert Einstein building (C2), Rabanales campus of the University of Cordoba (Spain, latitude: 37.85° N; longitude: 4.18° W).

In this way, the annual operation of the device at that location is simulated, considering three-minute intervals. In each of these 175,200-time instants ($175200 = (60/3) \cdot 24 \cdot 365$), the solar vector (Equation (1)) has been determined, checking whether the instant corresponds to day or night. Specifically, considering that $\overrightarrow{v_p}$ is the vertical vector of the location, given by Equation (15) as a function of latitude φ (Figure 1), it will be daytime if $\overrightarrow{v_p} \cdot \vec{s} > 0$.

$$\overrightarrow{v_p} = 0\vec{\imath} + cos\,\varphi\,\vec{j} + sin\,\varphi\,\vec{k}, \tag{15}$$

In addition, considering the dimensions of the device (Table 2), the distance $l_A - l_C$ of the device was determined for each day of the year (Figure 13). This distance is related to the angle of the polygon A'ABC at its vertex A and, consequently, to the orientation of the mirror.

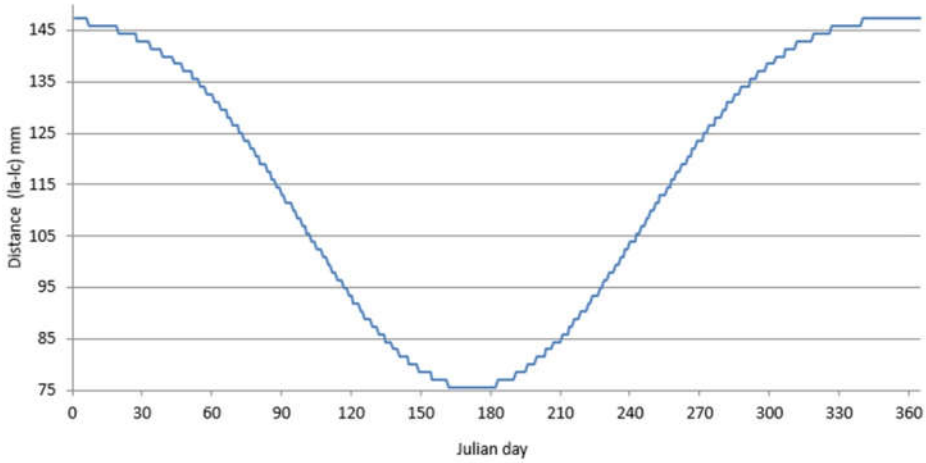

Figure 13. Evolution of $l_A - l_C$ versus Julian day.

Finally, the values of $\overrightarrow{n_a}$ (Equation (11)) and $\overrightarrow{n_p}$ (Equation (14)) have been generated for the time instants corresponding to the day. Under these conditions, it is possible to define the device approximation error, ε, as the angle between $\overrightarrow{n_a}$ and $\overrightarrow{n_p}$, which will be given for each time instant by Equation (16).

$$\varepsilon = arcos\left(\overrightarrow{n_a} \cdot \overrightarrow{n_p}\right), \tag{16}$$

From such approximation error, the pointing error will be the one formed by the reflected ray $\vec{r} = \vec{k}$ in the ideal situation where the heliostat is oriented perpendicular to $\overrightarrow{n_a}$ and the reflected ray in the real situation $\vec{r}'$ when the heliostat mirror is perpendicular to $\overrightarrow{n_p}$. As shown in Figure 14, according to the laws of reflection, the pointing error is twice the approximation error (Equation (17)).

$$\xi = (\alpha + \varepsilon) - (\alpha - \varepsilon) = 2\varepsilon, \tag{17}$$

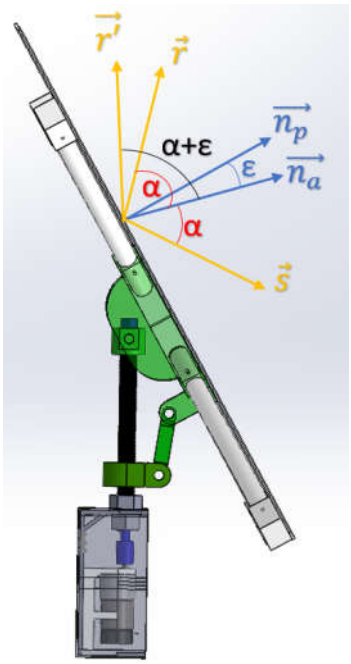

Figure 14. Geometric definition for pointing error ξ.

Thus, for each day of the year, a set of instantaneous pointing errors is obtained. Figure 15 shows the evolution of these errors for each month of the year.

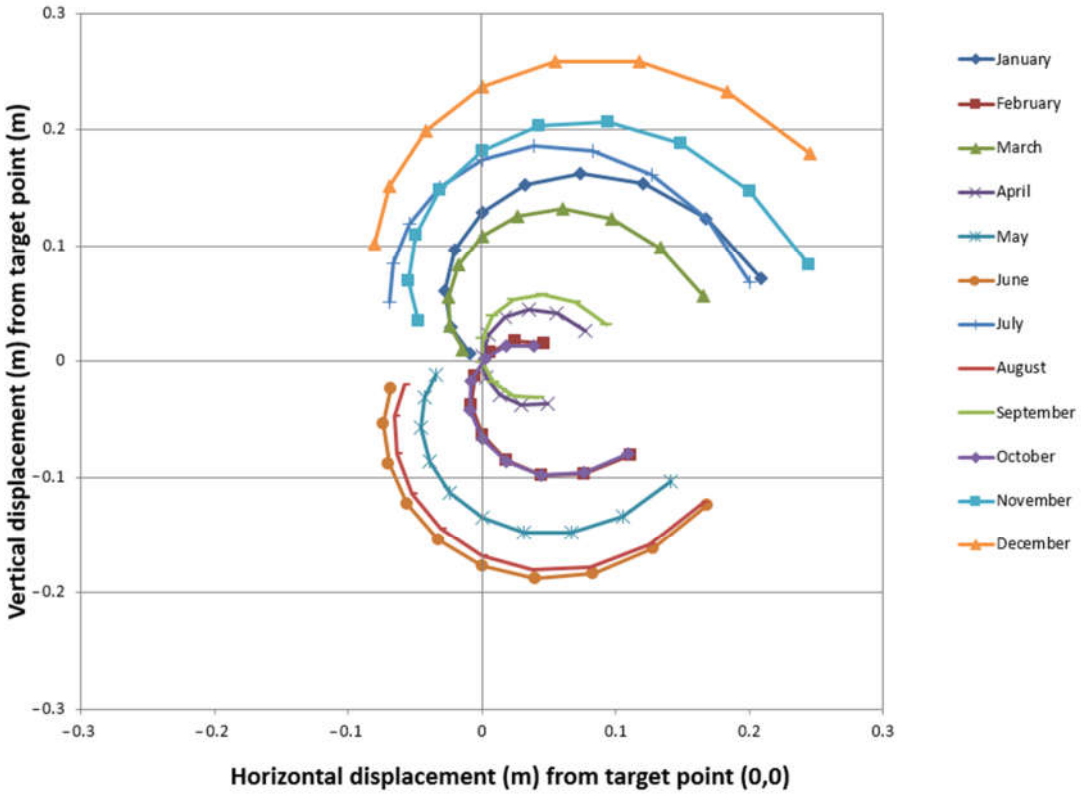

Figure 15. Monthly representation of pointing error ξ.

From these instantaneous errors, a classification has been made for each day of the year. Thus, Figure 16 shows the mean (Figure 16a) and maximum (Figure 16b) pointing errors for each Julian day and their evolution throughout the year.

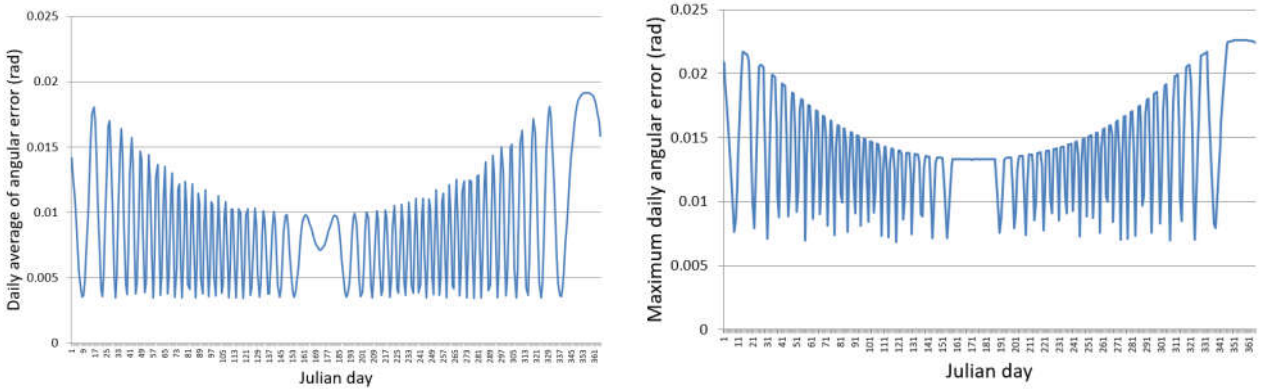

(**a**) (**b**)

Figure 16. Representation of pointing error ξ vs. Julian day: (**a**) mean pointing error; (**b**) maximum pointing error.

It is observed that the proposed heliostat is more accurate at positions with a high value of γ, corresponding to the summer solstice. However, the maximum values in winter are bounded by the maximum absolute error of 22 mrad. The overall errors are characterized by the histogram shown in Figure 17. It can be seen that there is a high probability that the error is less than 10 mrad, which implies, for real purposes, that the device can deflect the reflected beam up to 10 mm for each meter of distance between the heliostat and the focus. Thus, for a spotlight located 20 m away, the error will not exceed 20 cm, being very acceptable when this pointing occurs in the center of a window.

Figure 17. Frequency histogram of the proposed pointing error ξ.

4.2. Enhanced Heliostatic Illuminator: Improvements Achieved

According to the previously mentioned work, in this work an improved version of the single-axis polar heliostat proposed by Torres-Roldán et al. [45] is described.

Specifically, a new, more compact mechanical design has been developed to improve the stability and accuracy of the system. Likewise, the heliostat has been equipped with a direct transmission system that improves its movement. In addition, the system has been provided with a new mounting structure that greatly facilitates its correct installation for any desired orientation.

In addition, it has been manufactured using 3D technology with PETG, a plastic material that withstands the inclemencies typical of a device installed outdoors. Moreover, PETG is a plastic that can be recycled, which has an impact on the sustainability of the device presented. Furthermore, 3D printing significantly reduces the mass of the system. Specifically, while the heliostat proposed by Torres-Roldán et al. had a mass exceeding 35 kg, the new heliostatic illuminator has a mass of approximately 5 kg. This improvement, in the first instance, has an impact on its manageability. This reduction in mass, together with the new mounting structure, makes the heliostat installable by a single operator. It also has an impact on the stability of the system and its technical requirements, allowing the use of a lower cost motor. This, together with the cost of the plastic materials used, lowers production costs. Additionally, manufacturing by 3D printing facilitates its replicability. With all these improvements, the system daylighting is expected to be easily reproducible so that its implementation as a daylighting system can be extended.

5. Conclusions

One of the possible solutions to improve the energy efficiency of buildings consists of the installation of illuminating systems that increase the levels of natural lighting inside buildings, reducing energy consumption in artificial lighting. In line with this, it is worth mentioning the heliostatic illuminators that, although they can be complex systems, are very effective because they are equipped with a solar tracking system that increases the solar radiation used as natural lighting inside buildings. Accordingly, Torres-Roldán et al. [45] proposed a single-axis polar heliostat and analyzed its possible application as an illuminator [61]. However, this system suffers from important shortcomings that hinder its reproducibility and, consequently, its extensive implementation. In this work, an improved prototype of the single-axis polar heliostat proposed by Torres-Roldán et al. [45] is presented. Specifically, as has been discussed, the following improvements have been achieved:

- Mechanical design more compact and equipped with a direct transmission system that improves its movement;
- Significant reduction of the mass thanks to 3D manufacturing;
- Manufactured with recyclable and weather-resistant plastics;
- New structure for a more easy and precise installation;
- Greater stability and manageability;
- Lower production costs;
- Enhanced replicability.

Finally, in the present work an analysis of the pointing error of the proposed system has been performed, finding that the average pointing error is 10 mrad. This error implies a deviation of the reflected beam with respect to the target of only 10 mm for each meter of distance between the target and the heliostat. Thus, this error is acceptable in urban applications where these distances are around tens of meters. In this way, the proposed heliostat can improve the energy efficiency of buildings and contribute to the improvement of the sustainability of our cities and urban centers and the reduction of climate change. In line with this, future work will study and quantify the improvement in lighting conditions brought about by the installation of this type of lighting. The possible ways of user control over the illuminator as well as the levels of user acceptance and satisfaction will also be studied.

Author Contributions: Conceptualization, M.V.-M. and R.L.-L.; methodology, M.V.-M. and R.L.-L.; software, J.L.-S. and M.T.-R.; validation, J.L.-S. and J.C.R.-F.; formal analysis, R.L.-L. and L.M.F.-A.; investigation, J.L.-S., J.C.R.-F. and L.M.F.-A.; resources, M.T.-R. and L.M.F.-A.; data curation, L.M.F.-A. and J.C.R.-F.; writing—original draft preparation, J.L.-S. and M.V.-M.; writing—review and editing, R.L.-L. and M.V.-M.; visualization, J.L.-S. and J.C.R.-F.; supervision, R.L.-L. and M.V.-M.; project administration, R.L.-L. and J.C.R.-F.; funding acquisition, M.V.-M. and L.M.F.-A. All authors have read and agreed to the published version of the manuscript.

Funding: This research was funded by Programa Operativo FEDER Andalucía 2014–2020, grant number 1380888-R.

Data Availability Statement: Not applicable.

Conflicts of Interest: The authors declare no conflict of interest. The funders had no role in the design of the study; in the collection, analyses, or interpretation of data; in the writing of the manuscript; or in the decision to publish the results.

References

1. Dietz, T.; Shwom, R.L.; Whitley, C.T. Climate Change and Society. *Annu. Rev. Sociol.* **2020**, *46*, 135–158. https://doi.org/10.1146/annurev-soc-121919-054614.
2. Bernauer, T. Climate Change Politics. *Annu. Rev. Political Sci.* **2013**, *16*, 421–448. https://doi.org/10.1146/annurev-polisci-062011-154926.
3. Gupta, J. A history of international climate change policy. *WIREs Clim. Change* **2010**, *1*, 636–653. https://doi.org/10.1002/wcc.67.
4. United Nations. *Convención Marco de las Naciones Unidas Sobre el Cambio Climático*; United Nations: New York, NY, USA, 1992.
5. UNFCCC Report of the Conference of the Parties on Its Twenty-First Session, Held in Paris from 30 November to 13 December 2015. Part One: Proceedings; 2016; Volume 01192. Available online: https://unfccc.int/resource/docs/2015/cop21/eng/10.pdf (accessed on 14 December 2022).
6. IPCC Climate Change 2022: Impacts, Adaptation, and Vulnerability. Contribution of Working Group II to the Sixth Assessment Report of the Intergovernmental Panel on Climate Change; Cambridge, 2022. Available online: https://www.ipcc.ch/report/ar6/wg3/ (accessed on 14 December 2022).
7. United Nations The European Green Deal. Communication from the Commission; Brussels, 2019. Available online: https://www.esdn.eu/fileadmin/ESDN_Reports/ESDN_Report_2_2020.pdf (accessed on 14 December 2022).
8. Rivera, L. Necesidad de una Transición Energética Justa con las Personas y la Naturaleza; 2022. Available online: https://www.fundacioncarolina.es/wp-content/uploads/2022/10/DT_FC_OXFAM4.pdf (accessed on 14 December 2022).
9. Eurostat Shedding Light on Energy in the EU|2022 Interactive Edition; 2022. Available online: https://ec.europa.eu/eurostat/cache/infographs/energy/img/pdf/shedding-light-in-the-EU-2022_en.pdf?lang=en&lang=en (accessed on 14 December 2022).
10. Parlamento Europeo Directiva 2012/27/UE del Parlamento Europeo y del Consejo, de 25 de Octubre de 2012. D. of. la Unión Eur. 2012, pp. 1–56. Available online: https://eur-lex.europa.eu/eli/dir/2012/27/oj (accessed on 14 December 2022).
11. Kalinkina, N.; Zhdanova, I.; Chernysheva, I. The Organization of Natural Lighting in Buildings with Difficult Illuminated Areas; IOP Publishing Ltd: Bristol, England, 2020. https://doi.org/10.1088/1757-899x/753/3/032009.
12. Caicedo, D.; Pandharipande, A.; Willems, F.M. Daylight-adaptive lighting control using light sensor calibration prior-information. *Energy Build.* **2014**, *73*, 105–114. https://doi.org/10.1016/j.enbuild.2014.01.022.
13. Doulos, L.T.; Sioutis, I.; Tsangrassoulis, A.; Canale, L.; Faidas, K. Revision of Threshold Luminance Levels in Tunnels Aiming to Minimize Energy Consumption at No Cost: Methodology and Case Studies†. *Energies* **2020**, *13*, 1707. https://doi.org/10.3390/en13071707.
14. Alrubaih, M.S.; Zain, M.F.M.; Alghoul, M.A.; Ibrahim, N.L.N.; Shameri, M.A.; Elayeb, O. Research and development on aspects of daylighting fundamentals. Renew. *Sustain. Energy Rev.* **2013**, *21*, 494–505. https://doi.org/10.1016/j.rser.2012.12.057.
15. Yoo, S.; Kim, J.; Jang, C.-Y.; Jeong, H. A sensor-less LED dimming system based on daylight harvesting with BIPV systems. *Opt. Express* **2014**, *22*, A132–A143. https://doi.org/10.1364/oe.22.00a132.
16. Wong, I.L. A review of daylighting design and implementation in buildings. *Renew. Sustain. Energy Rev.* **2017**, *74*, 959–968. https://doi.org/10.1016/j.rser.2017.03.061.
17. Mohapatra, B.; Kumar, M.R.; Mandal, S.K. Positioning of light shelves to enhance daylight illuminance in office rooms. *Indones. J. Electr. Eng. Comput. Sci.* **2019**, *15*, 168–177. https://doi.org/10.11591/ijeecs.v15.i1.
18. Thongtha, A.; Boontham, P. Experimental Investigation of Natural Lighting Systems Using Cylindrical Glass for Energy Saving in Buildings. *Energies* **2020**, *13*, 2528. https://doi.org/10.3390/en13102528.
19. Jamala, N.; Rahim, R.; Shukri, S.M. The Architectural Analysis of the Illuminance Level in the Workspace, Using Natural and Artificial Lighting in Graha Pena Building in Makassar, Indonesia. *J. Des. Built Environ.* **2021**, *21*, 1–12. https://doi.org/10.22452/jdbe.vol21no1.1.

20. Berardi, U.; Wang, T. Daylighting in an atrium-type high performance house. *Build. Environ.* **2014**, *76*, 92–104. https://doi.org/10.1016/j.buildenv.2014.02.008.
21. Kwon, C.W.; Lee, K.J. Integrated Daylighting Design by Combining Passive Method with DaySim in a Classroom. *Energies* **2018**, *11*, 3168. https://doi.org/10.3390/en11113168.
22. Lee, K.S.; Han, K.J.; Lee, J.W. The Impact of Shading Type and Azimuth Orientation on the Daylighting in a Classroom–Focusing on Effectiveness of Façade Shading, Comparing the Results of DA and UDI. *Energies* **2017**, *10*, 635. https://doi.org/10.3390/en10050635.
23. Song, J.; Luo, G.; Li, L.; Tong, K.; Yang, Y.; Zhao, J. Application of heliostat in interior sunlight illumination for large buildings. *Renew. Energy* **2018**, *121*, 19–27. https://doi.org/10.1016/j.renene.2018.01.011.
24. Mayhoub, M. Innovative daylighting systems' challenges: A critical study. *Energy Build.* **2014**, *80*, 394–405. https://doi.org/10.1016/j.enbuild.2014.04.019.
25. Bystronski, Y. de A.; Martau, B.T.; Costa-Neto, W.I. Use of Light Pipe and Electronic Heliostat for Lighting of Underground Areas in Porto Alegre. In Proceedings of the SOLAR 2017 Conference; International Solar Energy Society, Freiburg, Germany, 9–12 October 2017; pp. 1–8.
26. Kontadakis, A.; Tsangrassoulis, A.; Doulos, L.; Zerefos, S. A Review of Light Shelf Designs for Daylit Environments. *Sustainability* **2018**, *10*, 71. https://doi.org/10.3390/su10010071.
27. Oakley, G.; Riffat, S.B.; Shao, L. Daylight Performance of Lightpipes. *Solar Energy* **2000**, *69*, 89–98.
28. Ikuzwe, A.; Sebitosi, A. A novel design of a daylighting system for a classroom in rural South Africa. *Sol. Energy* **2015**, *114*, 349–355. https://doi.org/10.1016/j.solener.2015.01.047.
29. Malet-Damour, B.; Boyer, H.; Fakra, A.; Bojic, M. Light Pipes Performance Prediction: Inter Model and Experimental Confrontation on Vertical Circular Light-guides. *Energy Procedia* **2014**, *57*, 1977–1986. https://doi.org/10.1016/j.egypro.2014.10.062.
30. Kennedy, D.M.; O'Rourke, F. Experimental analysis of a scaled, multi-aperture, light-pipe, daylighting system. *Sol. Energy* **2015**, *122*, 181–190. https://doi.org/10.1016/j.solener.2015.08.013.
31. Baroncini, C.; Boccia, O.; Chella, F.; Zazzini, P. Experimental analysis on a 1:2 scale model of the double light pipe, an innovative technological device for daylight transmission. *Sol. Energy* **2010**, *84*, 296–307. https://doi.org/10.1016/j.solener.2009.11.011.
32. Mohapatra, B.N.; Joshi, J. Modeling of vertical light pipes for daylight illumination of indoor industrial buildings. *Sci. Tech. J. Inf. Technol. Mech. Opt.* **2020**, *20*, 871. https://doi.org/10.17586/2226-1494-2020-20-6-871-876.
33. Jiménez-Valle, A.; Varo-Martínez, M.; López-Luque, R. Experimental regression model to predict natural lighting levels and energy savings in buildings. *Renew. Energy Power Qual. J.* **2016**, 537–541. https://doi.org/10.24084/rrepqj14.384.
34. Sreelakshmi, K.; Ramamurthy, K. Review on fibre-optic-based daylight enhancement systems in buildings. *Renew. Sustain. Energy Rev.* **2022**, *163*, 112514. https://doi.org/10.1016/j.rser.2022.112514.
35. Rosemann, A.; Kaase, H. Lightpipe applications for daylighting systems. *Sol. Energy* **2005**, *78*, 772–780. https://doi.org/10.1016/j.solener.2004.09.002.
36. Kischkoweit-Lopin, M. An overview of daylighting systems. *Sol. Energy* **2002**, *73*, 77–82. https://doi.org/10.1016/s0038-092x(02)00036-1.
37. Rosemann, A.; Mossman, M.; Whitehead, L. Development of a cost-effective solar illumination system to bring natural light into the building core. *Sol. Energy* **2008**, *82*, 302–310. https://doi.org/10.1016/j.solener.2007.09.003.
38. Tsangrassoulis, A.; Doulos, L.; Santamouris, M.; Fontoynont, M.; Maamari, F.; Wilson, M.; Jacobs, A.; Solomon, J.; Zimmerman, A.; Pohl, W.; et al. On the energy efficiency of a prototype hybrid daylighting system. *Sol. Energy* **2005**, *79*, 56–64. https://doi.org/10.1016/j.solener.2004.09.014.
39. Gibson, I.; Rosen, D.; Stucker, B.; Khorasani, M. *Additive Manufacturing Technologies*; Springer International Publishing: Cham, Switzerland, 2021. https://doi.org/10.1007/978-3-030-56127-7.
40. Akhadov, Z.Z.; Abdurakhmanov, A.A.; Sobirov, Y.B.; Kholov, S.R.; Mamatkosimov, M.A.; Kuchkarov, A.A. A system with a tracking concentrating heliostat for lighting underground spaces with beams of sunlight. *Appl. Sol. Energy* **2014**, *50*, 122–124. https://doi.org/10.3103/s0003701x14020030.
41. Ullah, I. Heliostats Daylighting System for Multi-floor Buildings. *J. Daylighting* **2019**, *6*, 202–209. https://doi.org/10.15627/jd.2019.18.
42. Yanpavlis, V.; Suzdalenko, A.; Stepanov, A.; Dzelzkaleja, L. Analysis of using a heliostat with non-rotating solar energy receivers. In Proceedings of the 2014 55th International Scientific Conference on Power and Electrical Engineering of Riga Technical University (RTUCON), Riga, Latvia, 14 October 2014; pp. 247–250. https://doi.org/10.1109/rtucon.2014.6998205.
43. Chang, C.-H.; Hsiso, H.-C.; Chang, C.-M.; Wang, C.-Y.; Lin, T.-H.; Chen, Y.-Y.; Lai, Y.-L.; Yen, C.-J.; Chen, K.-Y.; Whang, A.J.-W. Heliostat design for the daylighting system.. *Appl. Opt.* **2014**, *53*, H165–H169. https://doi.org/10.1364/ao.53.00h165.
44. Wang, C.-Y.; Whang, A.J.-W.; Tsai, Y.-L.; Yen, C.-J. The heliostat design for the Natural Light Illumination System. In Proceedings of the 2014 International Conference on Advanced Robotics and Intelligent Systems (ARIS), Taipei, Taiwan, 6–8 June 2014; pp. 103–106. https://doi.org/10.1109/aris.2014.6871500.
45. Torres-Roldán, M.; López-Luque, R.; Varo-Martínez, M. Design of an innovative and simplified polar heliostat for integration in buildings and urban environments. *Sol. Energy* **2015**, *119*, 159–168. https://doi.org/10.1016/j.solener.2015.06.041.
46. de Ahumada, L.F.; Physics for Energy and Renewable Resources Research Group. University of Cordoba. Spain; Torres-Roldán, M.; Osuna-Mérida, M.; Ramírez-Faz, J.; Luque, R.L.; Varo-Martínez, M. Daylighting system based on single-axis polar heliostat. *Renew. Energy Power Qual. J.* **2022**, *20*, 106–110. https://doi.org/10.24084/repqj20.235.

47. Fernández-Ahumada, L.M.; Osuna-Mérida, M.; López-Sánchez, J.; Gómez-Uceda, F.J.; López-Luque, R.; Varo-Martínez, M. Use of Polar Heliostats to Improve Levels of Natural Lighting inside Buildings with Little Access to Sunlight. *Sensors* **2022**, *22*, 5996. https://doi.org/10.3390/s22165996.
48. The third industrial revolution|Apr 21st 2012|The Economist. Available online: https://www.economist.com/weekly-edition/2012-04-21 (accessed on 9 November 2022).
49. Frank, A.G.; Dalenogare, L.S.; Ayala, N.F. Industry 4.0 technologies: Implementation patterns in manufacturing companies. *Int. J. Prod. Econ.* **2019**, *210*, 15–26. https://doi.org/10.1016/j.ijpe.2019.01.004.
50. Candi, M.; Beltagui, A. Effective use of 3D printing in the innovation process. *Technovation* **2019**, *80*, 63–73. https://doi.org/10.1016/j.technovation.2018.05.002.
51. Berman, B. 3-D printing: The new industrial revolution. *Bus. Horiz.* **2012**, *55*, 155–162. https://doi.org/10.1016/j.bushor.2011.11.003.
52. Weller, C.; Kleer, R.; Piller, F.T. Economic implications of 3D printing: Market structure models in light of additive manufacturing revisited. *Int. J. Prod. Econ.* **2015**, *164*, 43–56. https://doi.org/10.1016/j.ijpe.2015.02.020.
53. Huang, S.H.; Liu, P.; Mokasdar, A.; Hou, L. Additive manufacturing and its societal impact: a literature review. *Int. J. Adv. Manuf. Technol.* **2013**, *67*, 1191–1203. https://doi.org/10.1007/s00170-012-4558-5.
54. Bogers, M.; Hadar, R.; Bilberg, A. Additive manufacturing for consumer-centric business models: Implications for supply chains in consumer goods manufacturing. *Technol. Forecast. Soc. Change* **2016**, *102*, 225–239. https://doi.org/10.1016/j.techfore.2015.07.024.
55. Steenhuis, H.-J.; Pretorius, L. Consumer additive manufacturing or 3D printing adoption: an exploratory study. *J. Manuf. Technol. Manag.* **2016**, *27*, 990–1012. https://doi.org/10.1108/jmtm-01-2016-0002.
56. Petrovic, V.; Gonzalez, J.V.H.; Ferrando, O.J.; Gordillo, J.D.; Puchades, J.R.B.; Griñan, L.P. Additive layered manufacturing: sectors of industrial application shown through case studies. *Int. J. Prod. Res.* **2010**, *49*, 1061–1079. https://doi.org/10.1080/00207540903479786.
57. Beltagui, A.; Kunz, N.; Gold, S. The role of 3D printing and open design on adoption of socially sustainable supply chain innovation. *Int. J. Prod. Econ.* **2020**, *221*, 107462. https://doi.org/10.1016/j.ijpe.2019.07.035.
58. Delic, M.; Eyers, D.R. The effect of additive manufacturing adoption on supply chain flexibility and performance: An empirical analysis from the automotive industry. *Int. J. Prod. Econ.* **2020**, *228*, 107689. https://doi.org/10.1016/j.ijpe.2020.107689.
59. Gao, W.; Zhang, Y.; Ramanujan, D.; Ramani, K.; Chen, Y.; Williams, C.B.; Wang, C.C.L.; Shin, Y.C.; Zhang, S.; Zavattieri, P.D. The status, challenges, and future of additive manufacturing in engineering. *Comput. Aided Des.* **2015**, *69*, 65–89, doi:10.1016/j.cad.2015.04.001.
60. Spencer, W. Fourier series representation of the position of the Sun. *Search* **1971**, *2*, 172
61. Torres-Roldán, M.; López-Luque, R.; Varo-Martínez, M. Assessment of the pointing error of heliostats with a single not polar rotation axis for urban applications. *Sol. Energy* **2016**, *137*, 281–289. https://doi.org/10.1016/j.solener.2016.08.013.